Luminescent Eu3+-doped transparent alumina ceramics with high hardness

DRDLÍKOVÁ, K.; KLEMENT, R.; HADRABA, H.; DRDLÍK, D.; GALUSEK, D.; MACA, K.

Analog Integrated Circuits and Signal Processing
2017, vol. 37, iss. 14, pp. 4271-4277

ISSN : 0955-2219

DOI: http://dx.doi.org/10.1016/j.jeurceramsoc.2017.05.007

Accepted manuscript

Luminescent Eu^{3+}-doped transparent alumina ceramics with high hardness

Katarina Drdlikova[1], Robert Klement[2], Hynek Hadraba[3], Daniel Drdlik[1], Dusan Galusek[2], Karel Maca[1, 4]

[1] CEITEC BUT, Brno University of Technology, Purkynova 123, 612 00 Brno, Czech Republic

[2] Joint Glass Centre of the IIC SAS, TnU AD, and FCHFPT STU, Studentska 2, 911 50 Trencin, Slovakia

[3] CEITEC IPM, Institute of Physics of Materials, Academy of Sciences of the Czech Republic Zizkova 22, 616 62 Brno, Czech Republic

[4] Institute of Materials Science and Engineering, Brno University of Technology, Technicka 2, 616 69 Brno, Czech Republic

E-mail: katarina.drdlikova@ceitec.vutbr.cz

Abstract

The Eu^{3+}-doped transparent aluminas were prepared by wet shaping technique followed by pressure-less sintering and hot isostatic pressing. The effect of dopant amount on microstructure, real in-line transmission (RIT), photoluminescence (PL) properties, hardness and fracture behaviour was studied. The RIT decreased with increasing amount of the dopant. The PL emission spectra of Al_2O_3:Eu^{3+} ceramics exhibited predominant red light emission with the highest intensity (under 394 nm excitation) for material containing 0.125 at.% of Eu^{3+} and colour coordinates (0.645, 0.355) comparable with commercial red phosphors. The doping resulted in hardness increase from 26.1 GPa for undoped alumina to 27.6 GPa for Eu-doped

Corresponding author: Katarína Drdlíková, e-mail: katarina.drdlikova@ceitec.vutbr.cz

sample. The study of fracture surfaces showed predominantly intergranular crack propagation micro-mechanism.

Keywords

Alumina; europium; luminescence; transparent ceramics; mechanical properties

1. Introduction

Corundum (α-Al_2O_3) can be under certain conditions an optical material of great technological importance due to its high optical transparency in a wide spectral range from ultraviolet to near-infrared combined with excellent thermal stability, chemical inertness and good mechanical properties [1]. Contrary to its single crystal form (sapphire), submicron polycrystalline alumina ceramics exhibit even better mechanical properties which in combination with reasonable price could eventually lead to replacement of single crystals in optical applications.

It is well known that addition of rare-earth elements (RE) ions into various host materials results in an improvement of their structural, electronic and optical properties, expanding the areas of their use to various applications, including laser materials, optical amplifiers, phosphors, photocatalysts etc. [2-4]. Among the trivalent RE ions that exhibit characteristic f-f intraconfigurational narrow emission lines, the Eu^{3+} ion is a potential candidate for creation of luminescent materials due to its exceptional properties [5]. As trivalent cation, Eu^{3+} ion exhibits strong red monochromatic emission colour. For divalent Eu^{2+}, matrix tunable emission is ranging from blue to green spectral region. Thus, the Eu^{3+} ion has been frequently used as efficient luminescence probe due to its electronic/spectral properties [6]: (*i*) the excited $^5D_0$ state is well separated (~12,000 cm^{-1}) from $^7F_{0\text{-}6}$ states; (*ii*) $^5D_0$ and $^7F_0$ states are non-degenerate, so that $^5D_0 \rightarrow {}^7F_0$ transition exhibits a single peak when Eu^{3+} occupies only one site of symmetry type C_s, C_n, C_{nv} (proving the existence of more than one site of symmetry); (*iii*) long decay time (in millisecond range) from excited $^5D_0$ state; (*iv*) exceptionally large Stokes´ shift and (*v*) the intensity of $^5D_0 \rightarrow {}^7F_1$ transition (magnetic dipole in origin) is formally insensitive to the crystal field environment and consequently can be used as a reference transition. Moreover, the ligand-

to-metal charge transfer (LMCT) of Eu^{3+} corresponds to the reduction $4f^6 \rightarrow 4f^7L^{-1}$ and the Eu^{3+} tends to reduce in order to obtain the stable half-filled shell configuration [6, 7].

The Eu^{3+}-doped alumina was already prepared and characterized in the form of powders [8-10], microspheres [11] or in our previous work in the form of translucent ceramics [12]. Translucent Eu^{2+}-doped alumina (0.1 at.% Eu) was prepared and characterized by Yang et al. [13], who combined gel-casting and vacuum sintering and obtained the ceramics with in-line transmittance of 22% at 800 nm and typical blue light emission. In addition to our previously published results [12] this is to our best knowledge the only work dealing with europium doped transparent/translucent alumina. The lack of published data is primarily caused by the fact that the preparation of transparent luminescent ceramics is a major difficulty due to the significant decrease of optical transparency at higher dopant levels required for obtaining PL properties [14].

Unlike extensive studies of electronic, structural and optical properties of doped polycrystalline aluminas, investigation of their mechanical and/or fractographic properties is often neglected, and is largely limited to commonly used metallic dopants, such as magnesium [15, 16] or zirconium [16]. With exception of lanthanum-doped alumina, no reports on mechanical properties of RE-doped aluminas are available [17].

The main goal of this study was to enhance optical transparency of Eu^{3+}-doped alumina ceramics. Our previous work [18] reporting successful preparation of Er^{3+}-doped transparent alumina showed the highest PL intensity and transparency at the optimal dopant concentration of 0.1 at.%. Based on these results, the amount of Eu^{3+} dopant in the range of 0.05- 0.15 at.% was introduced into alumina using the optimised processing developed and described in our previous works [12, 18]. The second aim was to characterize the light emission, mechanical and fractographic properties of Eu^{3+}-doped aluminas and to discuss them in terms of dopant concentration and microstructure and to compare them with the data available in literature.

2. Experimental procedure

Commercial high purity Al_2O_3 powder (99.99%, TM-DAR, Taimei Chemicals Co., Japan) with the primary particle size of 150 nm was used as a base material. The Eu^{3+}-doped alumina samples were prepared according to optimised procedure as described in [12, 18] using Eu_2O_3 powder (purity 99.99%, particle size 30-50 nm, GNM – Getnanomaterials, USA). The final concentration of optically active dopant (Eu^{3+}) was in range to 0-0.15 at.% with respect to Al_2O_3.

Pressure-less sintering of green bodies was carried out to achieve 95.0-97.3% of theoretical density, i.e. only closed porosity was present. Two-stage pre-sintering regime (TSP) was used [12].

The sintered samples were hot isostatically pressed (HIP, ABRA Shirp, Switzerland) at 1280°C/3h in argon atmosphere and pressure of 200 MPa. The reference undoped alumina was HIPed at 1250°C/3h.

The density of sintered samples was determined according to the Archimedes' principle by double weighing in deionised water. The theoretical density was calculated from the theoretical densities of Al_2O_3 and Eu_2O_3 by the rule of mixtures.

Scanning electron microscopy (Lyra 3, Tescan, Czech Republic) was used to examine the microstructures of sintered bodies. The mean grain size (MGS) was determined by the linear intercept method using a correction factor of 1.56 [19]. Minimum of 200 grains were measured in order to obtain statistically robust set of data.

The real in-line transmission (RIT) of polished samples was determined using a non-polarized He–Ne laser (λ = 632.8 nm). RIT values were measured in at least five different positions for each sample and were related to constant thickness of 0.8 mm.

The excitation and emission fluorescence spectra were recorded using Fluorolog FL3-21 spectrometer (Horiba, USA) equipped with PMT (R928) detector. The Xe-lamp (450 W) was

used as an excitation source. To eliminate the second-order diffraction of the radiation source, a cut-off filter was used in the measurements. The luminescence spectra of studied samples presented herein were recorded at room temperature in front face mode and corrected for spectrometer response and lamp (except of excitation spectra).

One kilogram load indentations (20 measurements for each sample) were made on polished cross sections using an instrumented hardness tester (Z2.5/ZHU0.2, Zwick/Roel, Germany). The fracture toughness was calculated from Young's modulus E [MPa], hardness H [MPa], the indentation load P [N] and crack length c [m] as follows [20]:

$$K_{Ic} = \alpha \sqrt{\frac{E}{H}} \frac{P}{c^{\frac{3}{2}}}. \quad (1)$$

The calibration factor α [-] has a value of 0.018. The Vickers imprint diagonals and crack lengths were measured by confocal laser microscope (LS3100, Olympus, Japan). Elastic modulus was estimated for each individual hardness measurement from the slope of the unloading curve using the method described by Oliver and Pharr [21].

3. Results and discussion

3.1 Microstructure and real in-line transmission

Pre-sintering was carried out in order to prepare materials with only closed porosity, i.e. suitable for HIP. Higher content of Eu^{3+} suppressed densification, so the temperatures needed for pre-sintering of doped samples were slightly higher than that for pure alumina (Table 1). The same applies for the temperature of HIP (1280°C for doped samples, 1250°C for pure alumina).

All samples were HIPed to full density; any possible minimal differences in relative density could not be distinguished with the use of applied measuring method. The values of mean grain size of HIPed samples are summarized in Table 2. The microstructure of pure alumina was slightly coarser than in doped samples, which confirmed, similarly to another additives segregating preferably at grain boundaries – e.g. Mg, Zr, Y, Er [12, 22], the grain growth inhibiting effect of Eu doping. However, in terms of their influence on measured properties (RIT, photoluminescence, mechanical properties), all microstructures could be considered as similar.

Optical transparency of doped alumina decreased with increasing dopant content (Table 2). Up to 0.125 at.% of Eu^{3+}, the decrease was negligible and the RIT remained relatively high. However, the addition of 0.15 at.% of the dopant resulted in significant drop of transparency. This effect was attributed to the excess of the dopant segregated at grain boundaries and subsequent formation of second phase inclusions [23]. Taking into account the RIT values, 0.125 at.% of Eu^{3+} could be considered as the maximum content of dopant which still allows relatively high level of transparency in studied materials. This conclusion is closely related to the size of alumina matrix grains. The fine grained (submicron) microstructure results in a large grain boundary area capable of absorbing a relatively high amount of dopant.

3.2 Photoluminescence properties

The photoluminescence excitation (PLE) spectra of Eu^{3+}-doped α-Al_2O_3 (not shown here) were monitored at 613 nm and recorded in the spectral range from 220 to 590 nm. The PLE spectra exhibited the features typical for Eu^{3+} ions, i.e. the broad band and several sharp peaks between 320 to 600 nm. The intensive broad band (absorption assigned as charge transfer (CT)) extending from 230 to 350 nm with maxima at ~293 nm was associated with charge transfer transition (LMCT, spin and dipole allowed transition) in the Eu^{3+}–O^{2-} species and corresponded to the electronic transition from 2*p* orbital of O^{2-} ions to the empty 4f orbitals of Eu^{3+} ions (LMCT, $2p(O^{2-})\rightarrow 4f(Eu^{3+})$). The sharp lines in the longer wavelength region were assigned to the intra-configurational 4f-4f transitions of the Eu^{3+} ion: at 318 nm overlapped with LMCT ($^7F_0\rightarrow{}^5H_4$), 362 nm ($^7F_0\rightarrow{}^5D_4$), 380 nm ($^7F_0\rightarrow{}^5L_7$), 394 nm ($^7F_0\rightarrow{}^5L_6$), 413 nm ($^7F_0\rightarrow{}^5D_3$), 464 nm ($^7F_0\rightarrow{}^5D_2$) and 525 nm ($^7F_0\rightarrow{}^5D_1$). The $^7F_0\rightarrow{}^5L_6$ transition at 394 nm was the strongest 4f-4f transition in the excitation spectra.

The photoluminescence emission (PL) spectra of Eu^{3+} doped α-Al_2O_3 ceramics under excitation at 296 nm (charge transfer band) and 394 nm (4f-4f transition) are shown in Fig. 1. The PL spectra of studied samples exhibited five major emission bands attributed to intra-configurational 4f-4f transitions of the Eu^{3+} ions originating from $^5D_0\rightarrow{}^7F_J$ levels (J = 0, 1, 2, 3, 4): $^5D_0\rightarrow{}^7F_0$ (~577 nm, yellow), $^5D_0\rightarrow{}^7F_1$ (580-600 nm, orange), $^5D_0\rightarrow{}^7F_2$ (605-635 nm, red), $^5D_0\rightarrow{}^7F_3$ (640-660 nm, red) and $^5D_0\rightarrow{}^7F_4$ (675-715 nm, deep-red). The strongest $^5D_0\rightarrow{}^7F_2$ emission located at 613 nm, known as hypersensitive transition, originated from forced electric dipole transition was expected to occur when Eu^{3+} ion occupies the sites of non-inversion symmetry. The $^5D_0\rightarrow{}^7F_1$ was magnetic dipole transition and was relatively independent of the site symmetry and crystal field strength (environment) around Eu^{3+} ion [24, 25]. The origin of other observed transitions were described in detail by Binnemans and Tanner [24, 25]. All

observed $^5D_0 \rightarrow {}^7F_J$ transitions were broader than those found in the other oxide hosts, e.g. such as o-$EuAlO_3$ [26], YAG:Eu^{3+}, YAP:Eu^{3+} [27]. The broader emission bands were also observed in the PL spectra of Eu^{3+}-doped Al_2O_3 powders treated at temperatures below 1200°C [8, 28-30]. The broadened emission bands arising from $^5D_0 \rightarrow {}^7F_J$ transitions of Eu^{3+} ions were due to inhomogeneous line broadening of the transitions and were typical for disordered structures such as glassy (amorphous) phases. The broader nature of all observed transitions of Eu^{3+}-doped Al_2O_3 ceramics may imply that Eu^{3+} ions occupy the distribution of distorted sites of C_{3v} symmetry in Al_2O_3 hosts and/or the sites of the same or even lower symmetry (e.g. C_s) embedded in the disordered structure of grain boundaries in the Al_2O_3 ceramics.

The emission intensities of Eu^{3+}-doped Al_2O_3 under excitation at 296 nm (LMCT band) and Eu^{3+} concentration of 0.05, 0.075 at.% were almost identical (Fig. 1a). The maximum intensities of all transitions were observed at 0.1 at.% of Eu^{3+}. Further increase in Eu^{3+} concentration resulted in a decrease of the emission intensity and could be attributed to the concentration quenching due to the decrease in the Eu-Eu interatomic distance. The concentration dependence of emission intensities was more evident under direct excitation of 4f levels at 394 nm (Fig. 1b) and 464 nm (not shown). The red emission intensity increased with increasing Eu^{3+} concentration reaching the maximum at 0.125 at.% of Eu^{3+}. When the Eu^{3+} doping ratio was greater than 0.125 at.%, the luminescence intensity decreased as a consequence of concentration quenching. The comparison of intensities of the highest emission peak (613 nm) in the PL spectrum of the 0.125 at.% of Eu^{3+}-doped sample under different excitation wavelengths revealed that the intensity at 296 nm excitation increased by a factor of ~3 compared to excitation at 394 nm and by a factor of ~9 at 464 nm. For the lowest studied concentration of Eu^{3+} (0.05 at.%) this factor increased to ~5 (296 nm/394 nm) and ~17 (296 nm/464 nm). The excitation at lower wavelength (e.g. 296 nm) enables the use of these

materials as efficient red emitting phosphors even at significantly lower Eu^{3+} doping concentration without greater attenuation of emitted red light intensity.

To evaluate the material performance on colour luminescent emission, CIE chromaticity coordinates were evaluated adopting the standard procedures [31]. In general, the colour of any light source can be represented as an (*x*, *y*) coordinate in the colour space. The chromatic coordinates (*x*, *y*) were calculated as follows [32]: $x = X/(X+Y+Z)$ and $y = Y/(X+Y+Z)$ where *X*, *Y*, and *Z* are defined as $X = \int \overline{x}(\lambda)s(\lambda)d\lambda$; $Y = \int \overline{y}(\lambda)s(\lambda)d\lambda$; $Z = \int \overline{z}(\lambda)s(\lambda)d\lambda$; $\overline{x}(\lambda)$, $\overline{y}(\lambda)$, $\overline{z}(\lambda)$ are CIE *x*, *y* and *z* colour matching functions, respectively and $s(\lambda)$ is the spectrum (spectral power distribution) of a light source. The (*x*, *y*) values were calculated from corrected PL emission spectra under excitation at 296 and 394 nm. The values of colour coordinates, very similar for all Eu^{3+} concentrations, were found to be (0.645, 0.355) for 296 nm excitation and (0.647, 0.353) for 394 nm excitation and were very close to the "red" line. These values are comparable with the commercial red phosphors like Y_2O_3:Eu^{3+} (0.645, 0.347) and Y_2O_2S:Eu^{3+} (0.647, 0.343). The Eu^{3+}-doped Al_2O_3 ceramics can be thus regarded as potential red emitting phosphor material.

3.3 Mechanical properties

Mechanical properties of Eu^{3+}-doped transparent alumina samples were studied by instrumented Vickers indentation at 1 kg load. Besides quantifying the plasticity (Vickers hardness *HV*) from imprint size, the method allows also determination of elastic constant (indentation Young´s modulus E_{IT}) from the elastic part of the load-depth curve according to the Oliver and Pharr's approach [21]. The dependence of indentation Young´s modulus and Vickers hardness on Eu^{3+} content are shown in Fig. 2a and Fig. 3a, respectively. The Young´s modulus decreased with increasing Eu^{3+} content: in comparison to undoped alumina reference the E_{IT} decreased by 14% at 0.15 at.% of Eu^{3+} doping. The addition of 0.05 at.% of Eu^{3+}

increased the Vickers hardness by about 5%. Further increase in Eu^{3+} content to 0.15 at.% did not lead to any statistically significant change of *HV*.

The elastic and plastic properties of ceramics are functions of porosity, grain size and presence of secondary phases. While the differences in porosity between samples were negligible, the Young´s modulus and Vickers hardness were mainly affected by grain size refinement (see Table 2) and presence of Eu^{3+} ions at alumina grain boundaries as a major factor influencing the grain boundary strength.

The indentation Young´s modulus values of Eu^{3+}-doped alumina were compared with literature data [33, 34] (Fig. 2b). The Young´s modulus decreased with decreasing grain size due to substantial increase of the number of interfaces (grain boundaries and triple junction points). The data fitted by a linear fit yielded the slope of 1:0.8. The more pronounced decrease of Young´s modulus was found with the increasing Eu^{3+} content with the slope of 1:1.4 (see Fig. 2b). The more pronounced decrease of Young´s modulus of Eu^{3+}-doped samples can be attributed to the increased free volume in the interfacial region due to the presence of Eu^{3+}. Eu^{3+} ions could accumulate at the alumina grain boundaries in the form of free Eu^{3+} ions and/or nano-sized Eu oxide particles [23]. Our recent investigations of a similar material revealed that only free RE ions segregate at grain boundaries [18]; the RE oxide particles were not observed. The Eu^{3+} ions segregated at grain boundaries disabled the uniform distribution of elastic and plastic deformation between adjacent alumina particles. The Young´s modulus was determined from the slope of the linear section of un-loading part of the load-depth indentation curve. Indentation Young´s modulus of 97% dense Eu_2O_3 was determined to be 118.0 GPa by Quesada et al. [35], while indentation Young´s modulus of the undoped Al_2O_3 was determined to be 354.5 GPa in this work. The Eu^{3+} ions at the alumina grain boundaries prevented the recovery of elastic deformation and decreased the elastic response of doped alumina and thus the alumina was less stiff (see Fig. 2).

Strengthening of material through grain size refinement can be described by Hall-Petch relation, which for the Vickers hardness *HV* assumes the form:

$$HV = HV_0 \cdot \frac{k_y}{d^{0.5}}, \quad (2)$$

where HV_0 is resistance of the lattice to dislocation motion in term of Vickers hardness, k_y is the strengthening coefficient, and d is an average grain diameter. The literature hardness data for various transparent aluminas [15, 17, 33, 34, 36-40] are summarized in Fig. 3b and compared with the data from this study. The fit of the data by the Hall-Petch relation for alumina yielded the values $HV_0 = 16.3$ and $k_y = 3.5$. The undoped alumina prepared in this study achieved one of the highest *HV* values (26.15 GPa) out of all published data but still falls within the limits of data scatter. The addition of small amounts of Eu^{3+} formed an effective barrier for grain growth during sintering. As a consequence the increase of hardness of Eu^{3+}-doped alumina was observed. The decrease of hardness due to the increase of Eu^{3+} content was just slightly pronounced (marked by red arrow in Fig. 3b) in comparison with hardness decrease of La_2O_3 doped alumina reported by Biswas et al. [17] (marked by blue arrow in Fig. 3b). Eu^{3+} situated at grain boundaries served also as a barrier for plastic deformation extension between adjacent alumina grains. Observed growth of Vickers hardness between undoped alumina (26.1 GPa) and 0.05 at.% Eu^{3+}-doped alumina (27.6 GPa) was 1.5 GPa (5.4%) (see Fig. 3). Increase in hardness was caused by both grain refinement and Eu^{3+} presence at the grain boundaries. The change of hardness with further increasing Eu content was negligible.

The fracture resistance of Eu^{3+}-doped alumina was expressed in terms of the indentation fracture toughness. The indentation fracture toughness measurement can be used as comparative method of fracture toughness assessment in qualitatively similar materials, but not as an exact method for fracture toughness determination. Indentation fracture toughness of

Eu^{3+}-doped alumina slightly decreased with increasing Eu^{3+} content from 2.3 $MPa \cdot m^{-1/2}$ to 2.0 $MPa \cdot m^{-1/2}$ for undoped alumina to 0.15 at.% Eu^{3+}-doped alumina, respectively (Fig. 4a). The measured K_{IC} value depends on elastic-plastic characteristics (E, H) and length of cracks propagating from the corner of plastic indentation imprint (Eq. 1). Both the Young´s modulus (Fig. 4) and Vickers hardness (Fig. 3) decreased with increasing Eu^{3+} content so that the E/H ratio was almost constant irrespective of the Eu^{3+} concentration. Since the calibration factor α and indentation load P were kept constant, the values of indentation fracture toughness were determined by the indentation crack lengths which are summarised in Fig. 4b. The crack length increased with the Eu^{3+} content and can be explained by a grain cohesion weakening due to the presence of Eu^{3+} segregated at the grain boundaries.

The side view of propagating indentation crack in undoped alumina and in 0.15 at.% Eu^{3+}-doped alumina are shown in Figs. 5a, b. In both cases predominantly intergranular crack propagation was observed. The micrographs of open crack surfaces (Figs. 5c, d) show mainly intergranular fracture with transgranular failure of some individual grains both in doped and undoped aluminas. As documented by Nishiyama et al.[39] the fracture toughness of alumina is grain size independent.

4. Conclusions

Transparent Eu^{3+}-doped alumina ceramics were prepared and studied in terms of RIT, photoluminescence, hardness and fracture toughness. The relatively high RIT up to 57% was measured at low dopant concentration but slight decrease of the RIT was observed with increasing dopant amount up to 0.125 at.% of Eu^{3+}. Similarly, the highest emission intensity, observed under 394 nm excitation, was found for the sample containing 0.125 at.% of Eu^{3+}. Sharp decrease of transparency and emission intensity at higher dopant contents indicated this concentration as optimal in terms of luminescence properties, without negative influence on RIT. The emission spectra consisted of inhomogeneously broadened lines of $^5D_0 \rightarrow {}^7F_J$ transitions of Eu^{3+} ions with predominant emission in the red and deep red spectral region. The calculated values of colour coordinates (0.645, 0.355) were very close to "red" line and comparable with commercial phosphors. Vickers hardness of prepared materials were as high as 27.6 GPa with the maximal values in a lower dopant concentration range (0.05-0.075 at.%). The hardness increase was attributed to refinement of alumina matrix grains due to Eu^{3+} doping. Predominantly intergranular crack propagation was observed in both doped and undoped aluminas. Slight decline of indentation fracture toughness was explained by the lower grain boundary strength due to Eu^{3+} dopant segregation at the grain boundaries.

Acknowledgement

This work is part of the project 5SA14857, which has acquired the financial contribution from the EU Framework Programme for Research and Innovation Horizon 2020 within the scope of the Marie Sklodowska-Curie Actions co-financed by the South Moravian Region according to the Grant Agreement no. 665860.

The financial support of this work by the grant VEGA 1/0631/14, GAČR 15-06390S and SAS-MOST-JRP-2015-6 is also gratefully acknowledged. This research has also been financially supported by the Ministry of Education, Youth and Sports of the Czech Republic under the project CEITEC 2020 (LQ1601).

References

[1] O. Ozuna, G.A. Hirata, J. McKittrick, Luminescence enhancement in Eu^{3+}-doped alpha- and gamma-Al_2O_3 produced by pressure-assisted low-temperature combustion synthesis, Appl Phys Lett 84(8) (2004) 1296-1298.

[2] T. Aitasalo, J. Holsa, H. Jungner, M. Lastusaari, J. Niittykoski, Thermoluminescence study of persistent luminescence materials: Eu^{2+}- and R^{3+}-doped calcium aluminates, $CaAl_2O_4:Eu^{2+},R^{3+}$, J Phys Chem B 110(10) (2006) 4589-98.

[3] C. Feldmann, T. Justel, C.R. Ronda, P.J. Schmidt, Inorganic luminescent materials: 100 years of research and application, Adv Funct Mater 13(7) (2003) 511-516.

[4] N. Rakov, F.E. Ramos, G. Hirata, M. Xiao, Strong photoluminescence and cathodoluminescence due to f-f transitions in Eu^{3+} doped Al_2O_3 powders prepared by direct combustion synthesis and thin films deposited by laser ablation, Appl Phys Lett 83(2) (2003) 272-274.

[5] G. Blasse, B.C. Grabmaier, Luminescent Materials, Springer Berlin Heidelberg2012.

[6] C.A. Kodaira, H.F. Brito, O.L. Malta, O.A. Serra, Luminescence and energy transfer of the europium (III) tungstate obtained via the Pechini method, J Lumin 101(1-2) (2003) 11-21.

[7] W.M. Faustino, O.L. Malta, E.E.S. Teotonio, H.F. Brito, A.M. Simas, G.F. de Sa, Photoluminescence of europium(III) dithiocarbamate complexes: Electronic structure, charge transfer and energy transfer, J Phys Chem A 110(7) (2006) 2510-2516.

[8] M.A.F. Monteiro, H.F. Brito, M.C.F.C.M. Felinto, G.E.S. Brito, E.E.S. Teotonio, F.M. Vichi, R. Stefani, Photoluminescence behavior of Eu^{3+} ion doped into gamma- and alpha-alumina systems prepared by combustion, ceramic and Pechini methods, Micropor Mesopor Mat 108(1-3) (2008) 237-246.

[9] S. Kumar, R. Prakash, V. Kumar, G.M. Bhalerao, R.J. Choudhary, D.M. Phase, Surface and spectral studies of Eu^{3+} doped alpha-Al_2O_3 synthesized via solution combustion synthesis, Adv Powder Technol 26(4) (2015) 1263-1268.

[10] A. Das, V. Sharma, Synthesis and Characterization of Eu^{3+} doped α-Al_2O_3 nanocrystalline powder for novel application in latent fingerprint development, Adv Mater Lett 7(4) (2016) 100-150.

[11] D.G. Liu, Z.F. Zhu, Photoluminescence properties of the Eu-doped alpha-Al_2O_3 microspheres, J Alloy Compd 583 (2014) 291-294.

[12] K. Bodisova, R. Klement, D. Galusek, V. Pouchly, D. Drdlik, K. Maca, Luminescent rare-earth-doped transparent alumina ceramics, J Eur Ceram Soc 36(12) (2016) 2975-2980.

[13] Y. Yang, H. Wei, L.H. Zhang, K. Kisslinger, C.L. Melcher, Y.Q. Wu, Blue emission of Eu^{2+}-doped translucent alumina, J Lumin 168 (2015) 297-303.

[14] E.H. Penilla, Y. Kodera, J.E. Garay, Blue-green emission in terbium-doped alumina (Tb:Al_2O_3) transparent ceramics, Adv Funct Mater 23(48) (2013) 6036-6043.

[15] A. Krell, P. Blank, Grain-size dependence of hardness in dense submicrometer alumina, J Am Ceram Soc 78(4) (1995) 1118-1120.

[16] A. Krell, P. Blank, H.W. Ma, T. Hutzler, M.P.B. van Bruggen, R. Apetz, Transparent sintered corundum with high hardness and strength, J Am Ceram Soc 86(1) (2003) 12-18.

[17] P. Biswas, M.K. Kumar, K. Rajeswari, R. Johnson, U.S. Hareesh, Transparent sub-micrometre alumina from lanthanum oxide doped common grade alumina powder, Ceram Int 39(8) (2013) 9415-9419.

[18] K. Drdlíková, R. Klement, D. Drdlík, T. Spusta, D. Galusek, K. Maca, Luminescent Er^{3+} doped transparent alumina ceramics, J Eur Ceram Soc 37(7) (2017) 2695-2703.

[19] M.I. Mendelson, Average grain size in polycrystalline ceramics, J Am Ceram Soc 52(8) (1969) 443-446.

[20] G.R. Anstis, P. Chantikul, B.R. Lawn, D.B. Marshall, A critical-evaluation of indentation techniques for measuring fracture-toughness: I, Direct crack measurements, J Am Ceram Soc 64(9) (1981) 533-538.

[21] W.C. Oliver, G.M. Pharr, An Improved Technique for Determining Hardness and Elastic-Modulus Using Load and Displacement Sensing Indentation Experiments, J Mater Res 7(6) (1992) 1564-1583.

[22] K. Bodisova, D. Galusek, P. Svancarek, V. Pouchly, K. Maca, Grain growth suppression in alumina via doping and two-step sintering, Ceram Int 41(9) (2015) 11975-11983.

[23] L. Lallemant, N. Roussel, G. Fantozzi, V. Garnier, G. Bonnefont, T. Douillard, B. Durand, S. Guillemet-Fritsch, J.Y. Chane-Ching, D. Garcia-Gutierez, J. Aguilar-Garib, Effect of amount of doping agent on sintering, microstructure and optical properties of Zr- and La-doped alumina sintered by SPS, J Eur Ceram Soc 34(5) (2014) 1279-1288.

[24] K. Binnemans, Interpretation of europium(III) spectra, Coordin Chem Rev 295 (2015) 1-45.

[25] P.A. Tanner, Some misconceptions concerning the electronic spectra of tri-positive europium and cerium, Chem Soc Rev 42(12) (2013) 5090-5101.

[26] Y. Onishi, S. Adachi, Structural and Luminescence Properties of $EuAlO_3$ Ternary Compound and Al_2O_3-Eu_2O_3 Compositions, Ecs J Solid State Sc 4(12) (2015) R153-R158.

[27] H.C. Jung, J.Y. Park, G.S.R. Raju, J.H. Jeong, B.K. Moon, J.H. Kim, H.Y. Choi, Crystalline structure dependence of luminescent properties of Eu^{3+}-activated Y_2O_3-Al_2O_3 system phosphors, Curr Appl Phys 9 (2009) S217-S221.

[28] Y. Onishi, T. Nakamura, S. Adachi, Solubility limit and luminescence properties of Eu^{3+} ions in Al_2O_3 powder, J Lumin 176 (2016) 266-271.

[29] N. Rakov, G.S. Maciel, Photoluminescence analysis of alpha-Al_2O_3 powders doped with Eu^{3+} and Eu^{2+} ions, J Lumin 127(2) (2007) 703-706.

[30] P.A. Tanner, Z. Pan, N. Rakov, G.S. Maciel, Luminescence of Eu^{3+} in alpha-Al_2O_3 powders, J Alloy Compd 424(1-2) (2006) 347-349.

[31] C.B.o.t.C.I.d.L.E.c. Publication CIE no 17.4. International Lighting Vocabulary, Vienna, Austria, 1987.

[32] G.B. Stringfellow, Chapter 1 Materials Issues in High-Brightness Light-Emitting Diodes, in: G.B. Stringfellow, M.G. Craford (Eds.), Semiconduct Semimet, Elsevier1997, pp. 1-45.

[33] A. Krell, S. Schadlich, Nanoindentation hardness of submicrometer alumina ceramics, Mat Sci Eng a-Struct 307(1-2) (2001) 172-181.

[34] A. Belenky, I. Bar-On, D. Rittel, Static and dynamic fracture of transparent nanograined alumina, J Mech Phys Solids 58(4) (2010) 484-501.

[35] A. Quesada, A. del Campo, J.F. Fernandez, Sintering behaviour and translucency of dense Eu_2O_3 ceramics, J Eur Ceram Soc 34(7) (2014) 1803-1808.

[36] S.D. Skrovanek, R.C. Bradt, Microhardness of a fine-grain-size Al_2O_3, J Am Ceram Soc 62(3-4) (1979) 215-216.

[37] A. Krell, J. Klimke, T. Hutzler, Advanced spinel and sub-μm Al_2O_3 for transparent armour applications, J Eur Ceram Soc 29(2) (2009) 275-281.

[38] R.S. Mishra, C.E. Lesher, A.K. Mukherjee, High-pressure sintering of nanocrystalline gamma-Al_2O_3, J Am Ceram Soc 79(11) (1996) 2989-2992.

[39] N. Nishiyama, T. Taniguchi, H. Ohfuji, K. Yoshida, F. Wakai, B.N. Kim, H. Yoshida, Y. Higo, A. Holzheid, O. Beermann, T. Irifune, Y. Sakka, K. Funakoshi, Transparent nanocrystalline bulk alumina obtained at 7.7 GPa and 800 degrees C, Scripta Mater 69(5) (2013) 362-365.

[40] L. Lallemant, V. Garnier, G. Bonnefont, A. Marouani, G. Fantozzi, N. Bouaouadja, Effect of solid particle impact on light transmission of transparent ceramics: Role of the microstructure, Opt Mater 37 (2014) 352-357.

Figure captions

Fig. 1 Emission spectra of Eu^{3+}-doped Al_2O_3 transparent ceramics samples excited at λ_{exc} = 296 nm (a) and λ_{exc} = 394 nm (b), respectively.

Fig. 2 The dependence of Young´s modulus of Eu^{3+}-doped alumina ceramics on the dopant content (a) and mean grain size (b).

Fig. 3 The dependence of Vickers hardness of Eu^{3+}-doped alumina ceramics on the dopant content (a) and grain size (b).

Fig. 4 The dependence of indentation fracture toughness (a) and indentation crack length (b) of Eu^{3+}-doped alumina ceramics on the dopant content.

Fig. 5 Micrographs of propagating indentation cracks and open crack surfaces in (a, c) undoped alumina and (b, d) 0.15 at.% Eu^{3+}-doped alumina.

Table captions

Table 1. Pre-sintering regimes for individual samples and achieved relative densities.

Table 2. Mean grain size and real in-line transmittance of rare earth doped alumina after HIP.

Table 1

Eu^{3+} concentration (at.%)	TSP – regime [a)]	Relative density (%)
0	1380 °C → 1230 °C / 10 h	95.0
0.05	1440 °C → 1280 °C / 10 h	96.7
0.075	1440 °C → 1280 °C / 10 h	97.1
0.1	1440 °C → 1280 °C / 10 h	97.0
0.125	1440 °C → 1280 °C / 10 h	96.1
0.15	1470 °C → 1280 °C / 10 h	97.3

[a)] TSP – without dwell time in first step

Table 2

Eu^{3+} concentration (at.%)	Mean grain size (nm)	Standard deviation (nm)	RIT (%)
0	500	80	60.3
0.05	390	50	57.3
0.075	400	50	56.5
0.1	350	40	56.5
0.125	360	40	56.4
0.15	340	40	45.1

Fig. 1

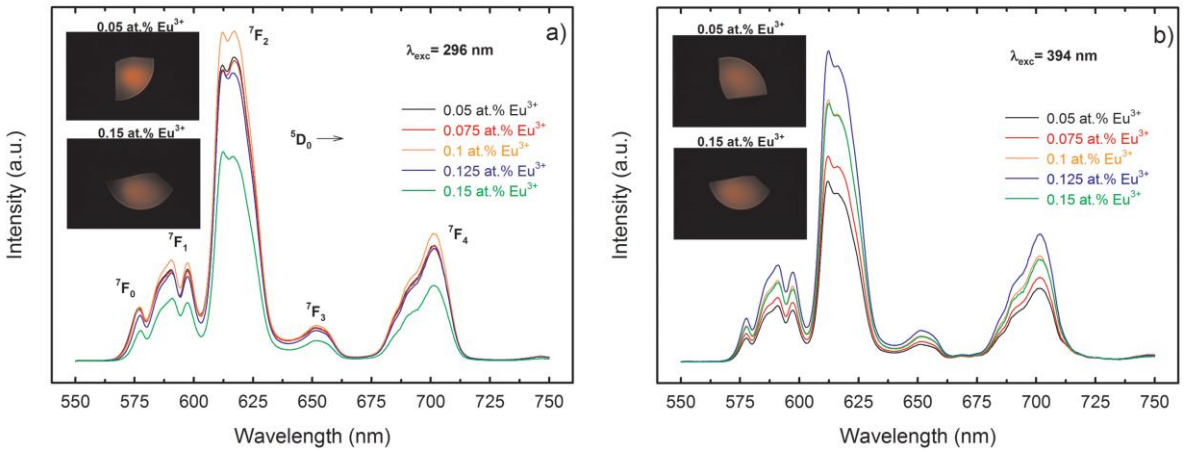
a)
b)
0.05 at.% Eu3+
0.15 at.% Eu3+
λexc= 296 nm
λexc= 394 nm
0.05 at.% Eu3+
0.075 at.% Eu3+
0.1 at.% Eu3+
0.125 at.% Eu3+
0.15 at.% Eu3+
7F0
7F1
7F2
7F3
7F4
5D0
Intensity (a.u.)
Wavelength (nm)
550 575 600 625 650 675 700 725 750

Fig. 2

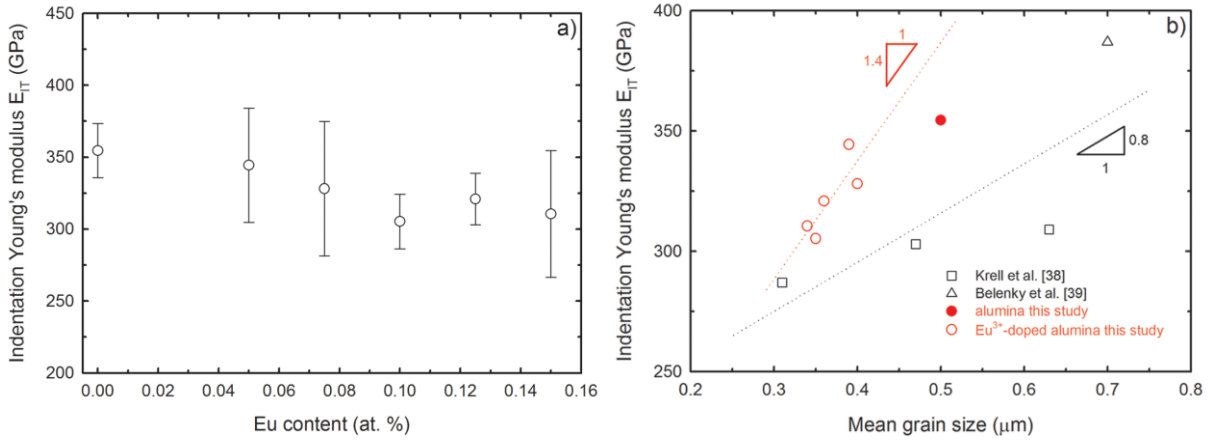
a)
Indentation Young's modulus E_{IT} (GPa)
Eu content (at. %)
b)
Mean grain size (μm)
1
1.4
0.8
1
Krell et al. [38]
Belenky et al. [39]
alumina this study
Eu^{3+}-doped alumina this study

Fig. 3

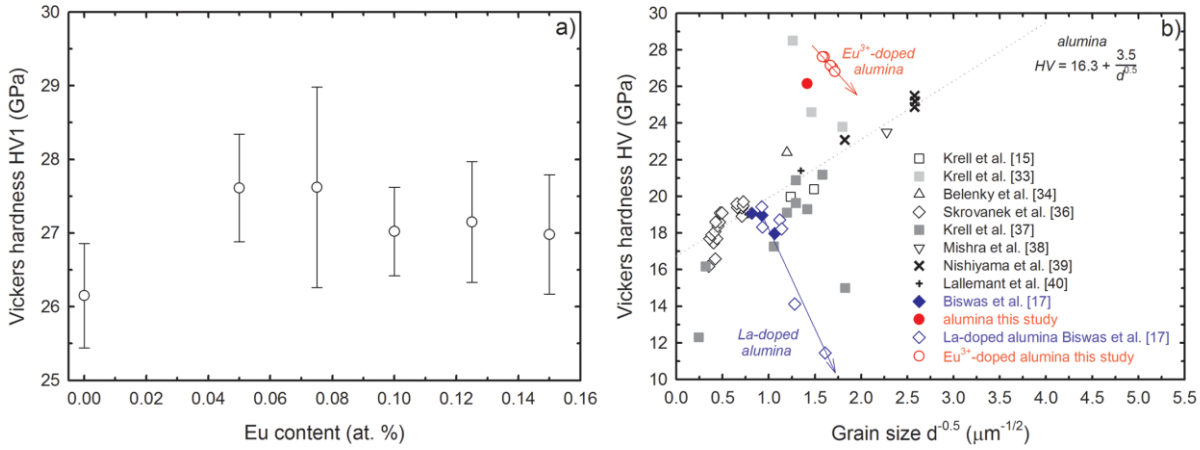
a)
Vickers hardness HV1 (GPa)
Eu content (at. %)
b)
Vickers hardness HV (GPa)
Grain size d^-0.5 (μm^-1/2)
alumina
HV = 16.3 + 3.5/d^0.5
Eu3+-doped alumina
La-doped alumina
Krell et al. [15]
Krell et al. [33]
Belenky et al. [34]
Skrovanek et al. [36]
Krell et al. [37]
Mishra et al. [38]
Nishiyama et al. [39]
Lallemant et al. [40]
Biswas et al. [17]
alumina this study
La-doped alumina Biswas et al. [17]
Eu3+-doped alumina this study

Fig. 4

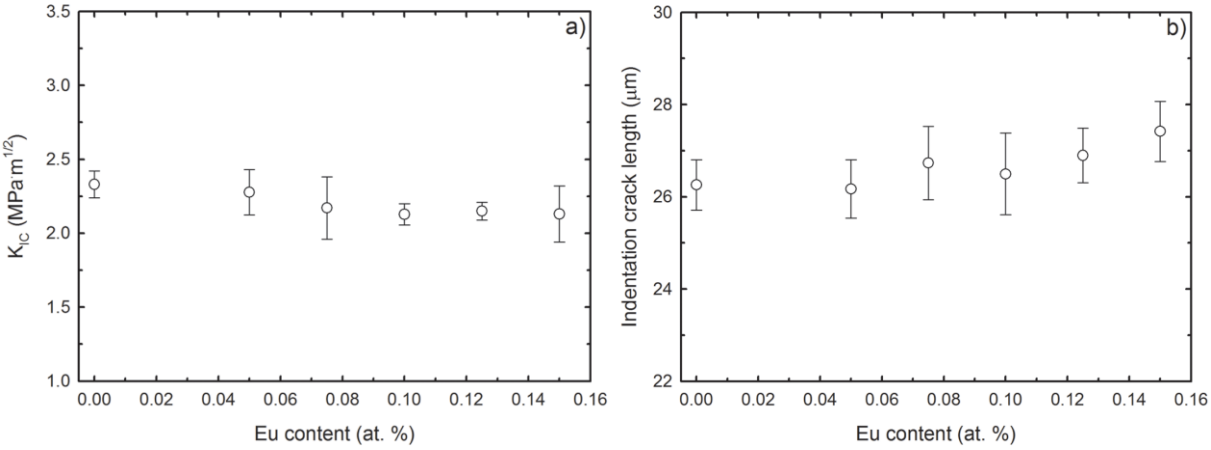
a)
b)
K_{IC} (MPa m$^{1/2}$)
Indentation crack length (μm)
Eu content (at. %)
Eu content (at. %)
3.5
3.0
2.5
2.0
1.5
1.0
30
28
26
24
22
0.00
0.02
0.04
0.06
0.08
0.10
0.12
0.14
0.16

Fig. 5